International Journal of Biological Macromolecules 322 (2025) 146868

Contents lists available at ScienceDirect

International Journal of Biological Macromolecules

journal homepage: www.elsevier.com/locate/ijbiomac

Sustainable reduction of Cr (VI) by green synthesized chitosan coated copper (II) nanoparticles in batch reactor system: Isotherm, thermodynamics and kinetic study

Veer Singh [a], Anurag Kumar Singh [b], Kumar Abhishek [c], Vikash Kumar [a], Ravi Ranjan [a], Shobha Kumari [a], Sonali Vedika [a], Ashiq Hussain Bhat [d], Vishal Mishra [e], Ashish Kumar [a,*]

[a] Department of Biochemistry, ICMR-RMRIMS, Agamkuan, Patna 800007, India
[b] Department of Pharmaceutical Engineering and Technology, IIT (BHU), Varanasi 221005, India
[c] DHR-Model Rural Health Research Unit, Kurhani, Muzaffarpur, Bihar, India
[d] Department of Bio-Statistics, ICMR-RMRIMS, Agamkuan, Patna 800007, India
[e] School of Biochemical Engineering, IIT (BHU), Varanasi 221005, India

ARTICLE INFO

Keywords:
Green synthesis
Chitosan coated Cu_2O nanoparticles
Cr (VI)
Adsorption

ABSTRACT

This study explores the use of green-synthesized chitosan-coated Cu_2O nanoparticle (Ch-CuNs) for the sustainable removal of hexavalent chromium (Cr (VI)). Scanning electron microscope (SEM) analysis confirmed the formation of spherical nanoparticles, while energy dispersive X-ray analyzer (EDX) and elemental analysis verified the presence of Cr (VI) on the nanoparticle surface, indicating successful adsorption. Fourier Transform Infrared (FTIR) spectroscopy analysis identified functional groups on the nanoparticles that actively participated in Cr (VI) adsorption. The specific surface area of Ch-CuNs was increased due coating of chitosan on nanoparticle surface. Freundlich isotherm model best fitted ($R^2 = 0.99$) and described multilayer adsorption of Cr (VI) onto Ch-CuNs. Pseudo-second-order model was best fitted for the adsorption process and this suggests that Cr (VI) adsorption was chemisorption. The thermodynamic parameters, with a positive enthalpy change ($\Delta H^\circ = 885.97$ J mol^{-1}) and entropy change ($\Delta S^\circ = 60.09$ J K^{-1} mol^{-1}), indicate that the adsorption process is endothermic and favourable. The results show that Ch-CuNs exhibit high Cr (VI) adsorption capacity (91.96 mg/g). In series reactor system, complete removal of Cr (VI) was achieved. This study highlights the potential of chitosan coated green-synthesized Ch-CuNs as effective and sustainable agents for removing Cr (VI) from contaminated water.

1. Introduction

Water contaminated with hexavalent chromium (Cr (VI)) is a serious environmental and public health concern [1]. Cr (VI) contamination in water arises from both natural and anthropogenic sources. Naturally, Cr (VI) forms through the oxidation of Cr (III) by manganese oxides in rocks like birnessite, asbolane, and lithiophorite [2]. Anthropogenic sources include industrial activities such as chromite ore processing, metal manufacturing, and improper disposal of waste, which lead to Cr (VI) leaching into water bodies [2]. In the U.S., Cr (VI) is also found in groundwater due to natural geochemical processes [3]. These sources contribute to widespread Cr (VI) pollution, posing significant health risks due to their carcinogenic properties [2]. World Health Organization (WHO) has established a maximum permissible limit of 0.05 mg/L for Cr (VI) in drinking water and surface water [4]. Exceeding this limit poses significant health risks, including cancer, kidney damage, liver damage, respiratory issues, skin problems, and other adverse effects. Due to the high toxicity of Cr (VI) to human health, its removal from water is crucial. Effective remediation strategies are essential to mitigate these risks and ensure safe drinking water. The WHO guidelines emphasize the importance of maintaining strict limits to protect public health [5,6].

Several physical and chemical methods are available for removing Cr (VI) from water, including reverse osmosis, ion exchange, and chemical precipitation. However, these techniques have drawbacks: they generate by-products or secondary pollutants, are operationally complex, and are costly to operate. For instance, reverse osmosis produces concentrated brine, while chemical precipitation generates sludge that requires

* Corresponding author.
E-mail address: ashish2k8@gmail.com (A. Kumar).

https://doi.org/10.1016/j.ijbiomac.2025.146868
Received 22 April 2025; Received in revised form 9 August 2025; Accepted 12 August 2025
Available online 13 August 2025

further treatment [7]. These limitations highlight the need for more sustainable alternative methods which offer high selectivity and reusability [8]. Hence, the an urgent requirement of eco-friendly, cost-effective and efficient methods to eradicate Cr (VI) from contaminated water. Due to the unique properties of nanoparticles, in particular their elevated surface area to volume ratio, nanotechnology holds potential for environmental remediation [9]. Ye et al. [10] investigated Cr (VI) removal from wastewater by Cu/Fe bimetallic nanoparticles. Among various nanoparticles, Cu_2O nanoparticles (CuNs) have attracted considerable interest for their potential applications in water treatment. However, conventional synthesis methods often involve toxic reagents that can be harmful to the environment [11]. Therefore, green synthesis approaches are considered eco-friendly and sustainable alternatives [12]. Tefera et al. [13] investigated Cr (VI) removal from wastewater by green synthesized cuprous oxide nanoparticles. Tefera et al. [13] did not report the surface modification of nanoparticles. In the present study, chitosan biopolymer was coated on the CuNs surface to enhance the Cr (VI) adsorption capacity.

In the current research, *Citrus limmeta* peel extract and chitosan biopolymer were employed for the synthesis of CuNs. Sweet lime (*Citrus limmeta*): A widely abundant agricultural waste product in India and can be used as a renewable source for the synthesis of nanoparticles [14]. Extracts from the peel are rich in bioactive compounds, for example, flavonoids, phenolics, and ascorbic acid, and these can serve as reducing agents when synthesizing nanoparticles [15]. Chitin, obtained from the exoskeleton of crustaceans, is a biopolymer that can be easily converted into chitosan, possessing excellent adsorption properties. Chitosan is a linear polymer of D-glucosamine and *N*-acetyl-D-glucosamine [16]. The hybridization of *Citrus limmeta* peel extract and chitosan offers a green approach for the synthesis of chitosan functionalized CuNs (Ch-CuNs) which lowers the environmental hazard during the synthesis [14]. Small particle size and presence of presence of the surface functional groups on Ch-CuNs, which took part in the enhanced Cr (VI) adsorption [10,16].

This study clearly shows the potential of green-synthesized Ch-CuNs for removing Cr (VI) from contaminated water as a novel and sustainable agent. The green synthesis method employing agricultural waste products and biopolymers is economical and eco-friendly for the synthesis of nanoparticles. Since the technology is less harmful, it can find more effective approaches to water treatment.

2. Material and methods

2.1. Synthesis of Ch-CuNs

Citrus limetta peels were collected from the local market in Patna, India. The peels were thoroughly washed with distilled water and dried in a hot air oven (Rescholar Equipment, Make India) at 50 °C for 48 h. The dried peels were then ground into a fine powder using a ball mill. *Citrus limetta* leaf extract was prepared from *Citrus limetta* peel powder. The peel powder (20 g) was boiled in 200 mL of distilled water for 4 h and then filtered using Whatman filter paper. 50 mL $CuSO_4{\cdot}5H_2O$ (ACS grade, ≥98.0 % purity was purchased from Sigma-Aldrich make USA) solution of 0.1 M was prepared separately. A 10 mL starch solution of 1 % was prepared, separately. Starch plays a dual role in the synthesis of Cu_2O nanoparticles as both a reducing agent and a stabilizing/capping agent. Starch Hi-AR™/ACS grade was purchased from HiMedia Laboratories Pvt. Ltd. India. 50 mL $CuSO_4{\cdot}5H_2O$, 40 mL *Citrus limetta* leaves extract and 10 mL starch solution were mixed and stirred continuously for 30 min at 80 °C. After stirring, 30 mL of 1 M sodium hydroxide (NaOH) (ACS grade, ≥98 % purity, Sigma-Aldrich make USA) was added, and the mixture was stirred for an additional 120 min. The colour of the solution turned blue to red-brown. The precipitated Cu_2O nanoparticles (CuNs) were collected and washed with distilled water. Post synthesis of CuNs, 5 g of CuNs were mixed to the 0.1 % chitosan (medium molecular weight, deacetylation degree ≥75 % from Sigma-Aldrich make USA) solution and kept in a rotary incubator shaker at 100 rpm and 37 °C, for 2 h. The synthesized chitosan-coated CuNs Ch-CuNs were subjected to centrifugation performed using a benchtop centrifuge (Thermo Scientific, USA) and washed with distilled water. The synthesized Ch-CuNs were dried in the oven at 50 °C for 24 h and stocked in an airtight box until further application.

2.2. Characterization of Ch-CuNs

The surface functional groups of Ch-CuNs were identified by Fourier Transform Infrared (FTIR) spectroscopy using the NICOLET iS5 instrument make USA. The Ch-CuNs surface morphology and elemental composition were then characterized by scanning electron microscope (SEM) (ZEISS MA15/18 make USA) and energy dispersive X-ray (EDX) (ZEISS MA15/18 make USA). Elemental mapping and surface composition analysis were performed using SEM-EDX. The oxidation state of chromium present on the surface of the CMNPs was observed through XPS (Thermo Fisher Scientific make, USA) analysis. The specific surface area and pore size were determined using the Brunauer–Emmett–Teller (BET) equation with a surface area analyzer (Tristar 3020, Micromeritics-II, Norcross, GA, USA). Pore size distribution was calculated using the Barrett–Joyner–Halenda (BJH) method. The total pore volume was estimated from the amount of nitrogen (N_2) adsorbed at a relative pressure (P/P_o) of 0.99.

X-ray diffraction (XRD) study of chitosan powder, CuNs and Ch-CuNs was done using a Rigaku Miniflex 600 Desktop X-Ray Diffraction System make Tokyo, Japan. The zero point charge (pHzpc) of the Ch-CuNs was established by a conventional method. In separate 100 mL conical flasks, 50 mL of 0.1 M potassium nitrate (KNO_3) solution was transferred, and the initial pH values were adjusted within the 2–10 range by adding either 0.1 N HCl or 0.1 N NaOH. KNO_3 analytical reagent (AR) grade, ≥99 % purity was obtained from HiMedia Laboratories Pvt. Ltd. (India). 0.1 g of Ch-CuNs was added into each flask and incubated for 24 h at 37 °C, 120 RPM in the rotator incubator shaker (REMI CIS-24 BL make India). The final pH values of the supernatant were determined and the graph between pH_{final}-$pH_{initial}$ vs pH_{final} to estimate the pH_{zpc} of the Ch-CuNS [17,18].

2.3. Cr (VI) adsorption study

500 mL of 1000 mg/L Cr (VI) solution was prepared from potassium dichromate ($Cr_2K_2O_7$) purchased from Sigma-Aldrich make USA. The adsorption experiment was performed using a 50 mL working solution (0.25 g/L Cr (VI), pH 2). The study explored the influences of temperature (20–50 °C), contact time (60–360 min), stirring speed (120–300 rpm), solution pH (2−10), initial Cr(VI) concentration (25–100 mg/L) and Ch-CuNs dosage (0.25–1.0 g/L) on Cr(VI) adsorption by Ch-CuNs. At the end of the adsorption process, water samples were taken from the flask and centrifuged at 5000 rpm for five minutes. The remaining Cr (VI) in the water was measured using 1, 5-Diphenylcarbazide at 540 nm. Absorbance measurements were carried out using a UV–visible spectrophotometer (Make: Shimadzu, Japan).

The percentage removal of Cr (VI) and the adsorption capacity (qe) of Ch-CuNs were determined using Eqs. (1) and (2) [19]. These equations allow for the calculation of the percentage removal and the amount of Cr (VI) adsorbed per unit mass of adsorbent.

$$\text{Removal}(\%) = \frac{C_i - C_e}{C_i} \times 100 \tag{1}$$

$$q_e = \frac{(C_i - C_e) \times V}{W} \tag{2}$$

where Ci and C_e are the initial and equilibrium concentrations of Cr (VI) (mg/L), V is the volume of the Cr (VI) solution (L), and W is the weight of the Ch-CuNs (g).

The isotherms, thermodynamics and kinetic study were performed to explain the behaviour of Cr (VI) adsorption. These studies have been

mentioned in the Sections S1-S3 of supplementary data [20–25].

Desorption of Cr (VI) and regeneration of adsorbent study were performed. The desorption study is provided in the Section S4 of supplementary data.

2.4. Statistical data analysis

All adsorption experiments were conducted in triplicate ($n = 3$), and the mean values obtained were used to plot the graphs. The experimental errors were calculated as ± standard deviation and are represented as error bars in the graphs. For modeling purposes, the residual sum of squares (RSS) was employed as an error function, as described by Eq. (3).

$$RSS = \sum_{i=1}^{n} (qe.calc - qe.\exp)^2 \quad (3)$$

where, qe. *calc* and *qe. exp* are the calculated and experimental values of q_e and n is the number of experiments.

The calculated (qe. *Calc)* and experimental (*qe. exp*) values of the adsorption capacity were compared across n experiments.

To determine whether differences in Cr (VI) removal, across the levels of each parameter were statistically significant, a one-way analysis of variance (ANOVA) was performed. This test will be applied individually for each parameter. A p-value less than 0.05 indicates that there are significant differences of Cr (VI) removal means across different parameter values.

In addition, Pearson correlation analysis will be performed to assess the strength and direction of the linear relationship between each parameter and Cr (VI) removal. The correlation coefficient (r) quantifies the degree to which each parameter influence Cr (VI) removal, with values ranging from −1 (strong negative correlation) to +1 (strong positive correlation). The accompanying p-value from the test will be used to determine the statistical significance of the correlation. A p-value less than 0.05 indicates that the relationship was statistically significant and unlikely to have occurred by chance. This analysis provides important insights, whether Cr (VI) removal consistently increases or decreases with changes in each parameter value.

Together, these statistical techniques provide a comprehensive understanding of how each parameter independently influence the Cr (VI) removal and support the identification of optimal conditions for maximum removal.

In addition, a repeated measures analysis of variance (RM-ANOVA) was performed to determine whether differences in Cr (VI) adsorption and desorption across multiple cycles. This test was chosen because the same adsorbent material (Ch-CuNs) was used across successive cycles, resulting in dependent observations. RM-ANOVA accounts for within-subject variability and evaluates whether the change in Cr (VI) adsorption and desorption over cycles was statistically significant. A p-value less than 0.05 indicates that there are statistically significant differences in Cr (VI) adsorption and desorption across the regeneration cycles.

3. Results and discussion

3.1. Characterization of Ch-CuNs

3.1.1. FTIR analysis

FTIR analysis was used for identifying functional groups on the Ch-CuNs by generating an infrared absorption spectrum. The FTIR spectra of chitosan, CuNs, Ch-CuNs and Cr (VI)-loaded Ch-CuNs are shown in Fig. 1.

The broad bands in the 3000–3700 cm^{-1} region (Fig. 1) are characteristic of O—H and N—H stretching of hydrogen bonds in proteins, phenols, and alcohols [26]. The peak between 1500 and 1700 cm^{-1} indicates the C≡C stretching in aromatic rings [27]. Peaks between 1320 and 1350 cm^{-1}, are attributed to N—O symmetric stretching of

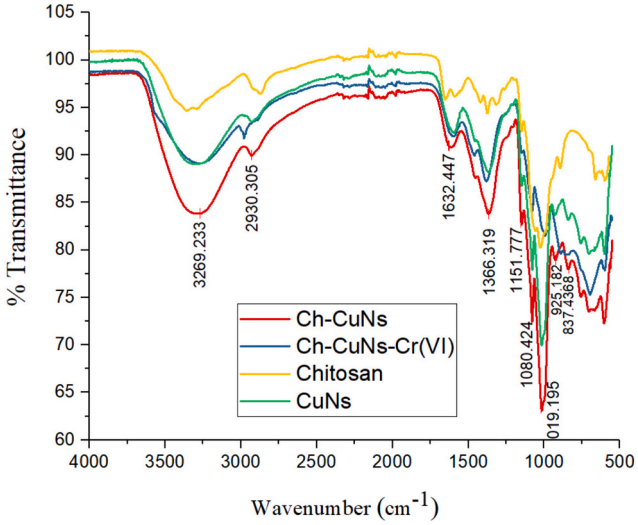

Fig. 1. FTIR spectra of chitosan, CuNs, Ch-CuNs and Cr (VI)-loaded Ch-CuNs.

groups containing nitrogen [28]. Peaks from 900 to 1100 cm^{-1} are attributed to C—O stretching of alcoholic groups, and the peak at 1147.48 cm^{-1} is associated with C—O stretching of ethers and lactones [29,30]. The FTIR spectra of chitosan were found to differ from CuNs. Lodging of Cr (VI) onto Ch-CuNs caused variations in the FTIR spectra, especially at 1147.48 cm^{-1} as well as between 900 and 1100 cm^{-1}. The FTIR results indicated the surface modification of Ch-CuNs with several functional groups such as -NH_2, -OH, C≡C, and C—O by chitosan modification. These functional groups played an important role in the Cr (VI) adsorption [31]. Al-Naamani et al. [32] performed Cr (VI) adsorption study by chitosan-ZnO nanocomposites and reported similar kinds of observation.

3.1.2. SEM-EDX

HR-SEM analysis was used to study the surface morphology of CuNs, Ch-CuNs and Cr (VI) loaded Ch-CuNs. Such surface properties, such as surface roughness or smoothness is key factors in the uptake of Cr (VI) [33]. Fig. 2 represents HR-SEM and EDX analysis of CuNs, Ch-CuNs and Cr (VI) loaded Ch-CuNs.

As shown in Fig. 2a, c and e, CuNs and Ch-CuNs were spherical in size. Moreover, the SEM images show a rough surface morphology that, coupled with their small size, increases their Cr (VI) adsorption properties. As compared to CuNs (Fig. 2a) the surface of Ch-CuNs (Fig. 2c) becomes porous and morphologically uneven due to the chitosan coating [34]. There is no clear changes were observed between Ch-CuNs (Fig. 2c) and Cr (VI) loaded Ch-CuNs (Fig. 2e). The surface roughness and porosity characteristics of Ch-CuNs are responsible for enhanced Cr (VI) adsorption ability and are considered to be suitable adsorbent agents. Khalil et al. [35] performed SEM analysis of chitosan-CuO nanocomposites and reported a similar kind of nanoparticle surface morphology.

Elemental analysis of CuNs (Fig. 2b), Ch-CuNs (Fig. 2d) and Cr (VI) loaded Ch-CuNs (Fig. 2f) was performed to confirm the presence of Cu, O, C and O elements. Cu and O are the major elements involved in the synthesis of CuNs and Ch-CuNs [36,37]. The presence of Cr (VI) on the surface of Ch-CuNs after adsorption was confirmed to the successful adsorption of Cr (VI). Muhammad et al. [38] reported the removal of Cr (VI) and Ni (II) using polyaniline, iron oxide and their composite materials. They used EDX analysis to verify the elemental compositions of these materials, and their results were similar to those mentioned in the previous studies. The EDX performance revealed elements associated with the adsorption properties of Ch-CuNs. This synthesis ability and elemental composition of Ch-CuNs are more suitable for adsorption applications.

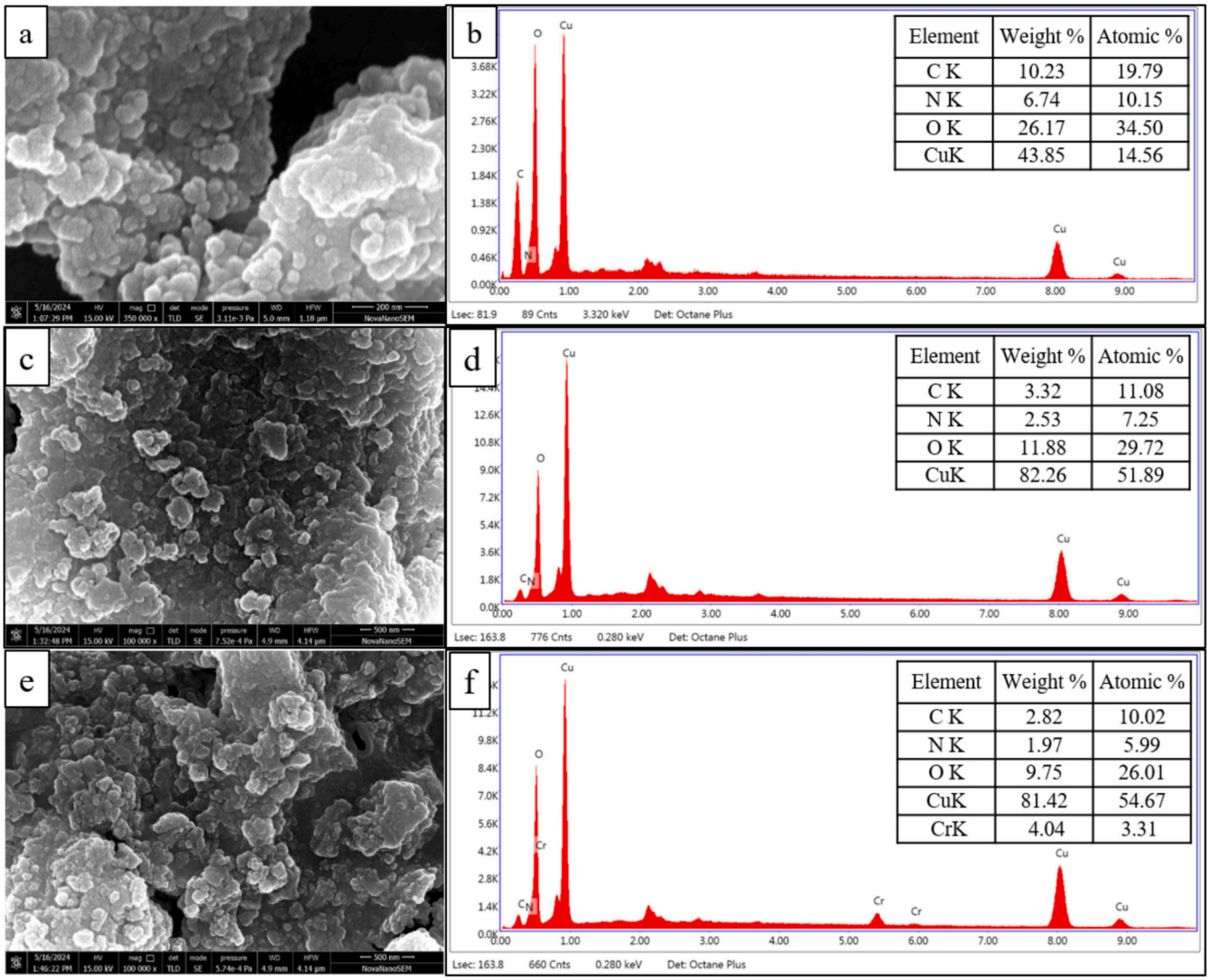

Fig. 2. SEM-EDX analysis of CuNs (a,b), Ch-CuNs (c,d) and Cr (VI) loaded Ch-CuNs (e,f).

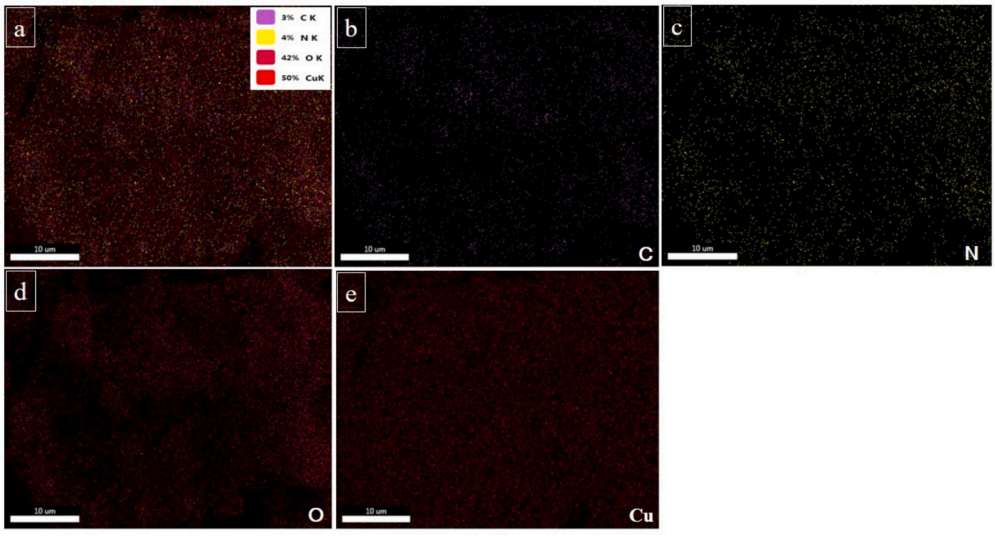

Fig. 3. Elemental mapping of C (b), N (c), O (d) and Cu (e) on Ch-CuNs before Cr (VI) adsorption.

3.1.3. Elemental mapping

The adsorbent surface was characterized by element mapping that either showed the absence or presence of such elements. The elemental mapping of Ch-CuNs before and after the adsorption of Cr (VI) is shown in Figs. 3 and 4.

From the elemental mapping (Fig. 3), it is evident that C, O, Cu and N were strongly expressed in the Ch-CuNs. The abundance of C and O contributed to the suitability of Ch-CuNs as an adsorbent for Cr (VI) removal. The presence of Cu indicated the successful formation of copper nanoparticles. In addition, the surface functional groups, e.g. -NH_2, created by the chitosan coating showed a high increase in nitrogen content. As exhibited by elemental mapping results, the distribution of Cr (VI) on the Ch-CuNs surface after adsorption was uniform distribution. The presence of the Cr (VI) on the adsorbent surface confirmed to the adsorption of Cr (VI) on the Ch-CuNs surface. Dinh et al. [39] reported similar findings in their elemental mapping of chitosan-MnO_2 nanocomposite.

3.1.4. Point of zero charge (pH_{zpc})

According to Mushtaq et al. [40], the pH at the pH_{ZPC} is an indicator of H^+ or OH^- on the surface of the adsorbent. Below the pH_{ZPC}, the adsorbent surface maintains a positive charge, while above it the surface turns negative [41]. As for the pH_{ZPC} of Ch-CuNs, it was calculated and depicted in Fig. 5.

The pH_{ZPC} of the Ch-CuNs was measured by adding to a dilute suspension of the nanomaterials at 0.5 g/L, giving a pH_{ZPC} of 6.21 (Fig. 5). At a pH below this point, the surface carries a positive charge, which facilitates the adsorption of negatively charged species, such as Cr (VI). At pH values above 6.21, the surface charge is negative and favourable for the adsorption of positive ions. This pH_{ZPC} value must be considered in the optimization of the adsorption process for efficient removal of Cr (VI.

The pH_{ZPC} led to the conclusion that at lower pH Cr (VI) chelates satisfactorily to the surface of the Ch-CuNs with the greater removal efficiency obtained at pH 2. The presence of $HCrO_4^-$ ions [41], and the positively charged (protonated) surface of Ch-CuNs attracted these negatively charged chromate ions [42]. Li et al. [43] studied the adsorption of Cu (II), Pb (II), and Cd (II) ions onto DTPA-modified magnetic graphene oxide. The adsorption of these heavy metal ions was more efficient at acidic pH levels, according to the study.

3.1.5. BET

Nitrogen adsorption-desorption isotherms were measured to estimate the surface area and average pore diameter of CuNs and Ch-CuNs (Fig. 6).

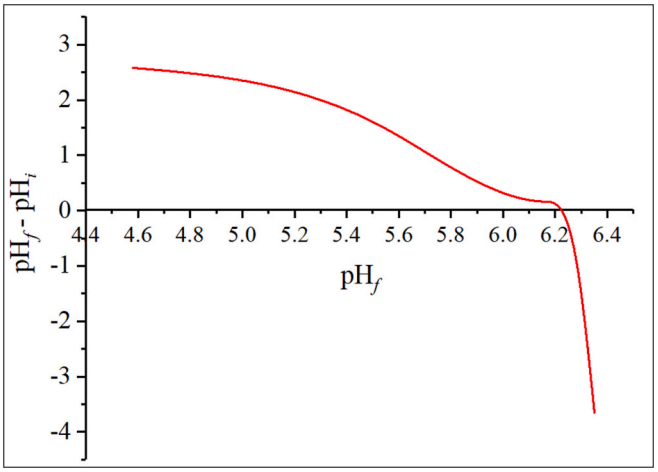

Fig. 5. pH_{zpc} value of Ch-CuNs.

This analysis also aided in confirming the chitosan coating on CuNs and characterizing their mesoporous structure. The results demonstrated uniform mesoporous channels and a narrow pore size distribution. The pore volume and surface area of CuNs were found to be 0.025 cm^3/g and 14.6 m^2/g, respectively. In contrast, the chitosan-coated CuNs (Ch-CuNs) exhibited a pore volume of 0.113 cm^3/g and a surface area of 34.45 m^2/g (Fig. 6). The Barrett–Joyner–Halenda (BJH) method confirmed average pore radii of 3.41 nm for CuNs and 6.57 nm for Ch-CuNs. These results indicate that chitosan coating significantly increased the surface area of the adsorbent. Zhang et al. [44] investigated the BET analysis of chitosan functionalized nanomaterials and reported that the surface area of nanoparticles was enhanced after chitosan coating.

3.1.6. XRD

XRD patterns of the chitosan and chitosan nanoparticles are obtained, and the corresponding results are presented in Fig. 7.

As shown in Fig. 7, chitosan displayed a strong diffraction peak at around 21°, which is associated with the mixture of (001) and (100) planes that belong to the monoclinic system [45]. XRD of CuNs and Ch-CuNs displayed a peak at 35°. To compare with the XRD spectrum of chitosan powder diffraction peak disappeared completely, the 35° diffraction peak relative intensity decreased significantly, and the

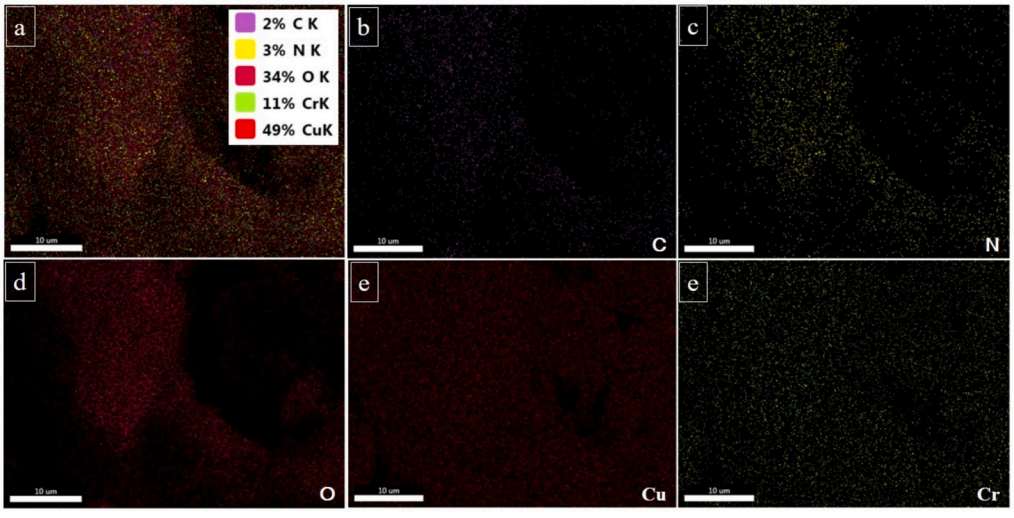

Fig. 4. Elemental mapping of C (b), N (c), O (d), Cu (e) and Cr (f) on Ch-CuNs after Cr (VI) adsorption.

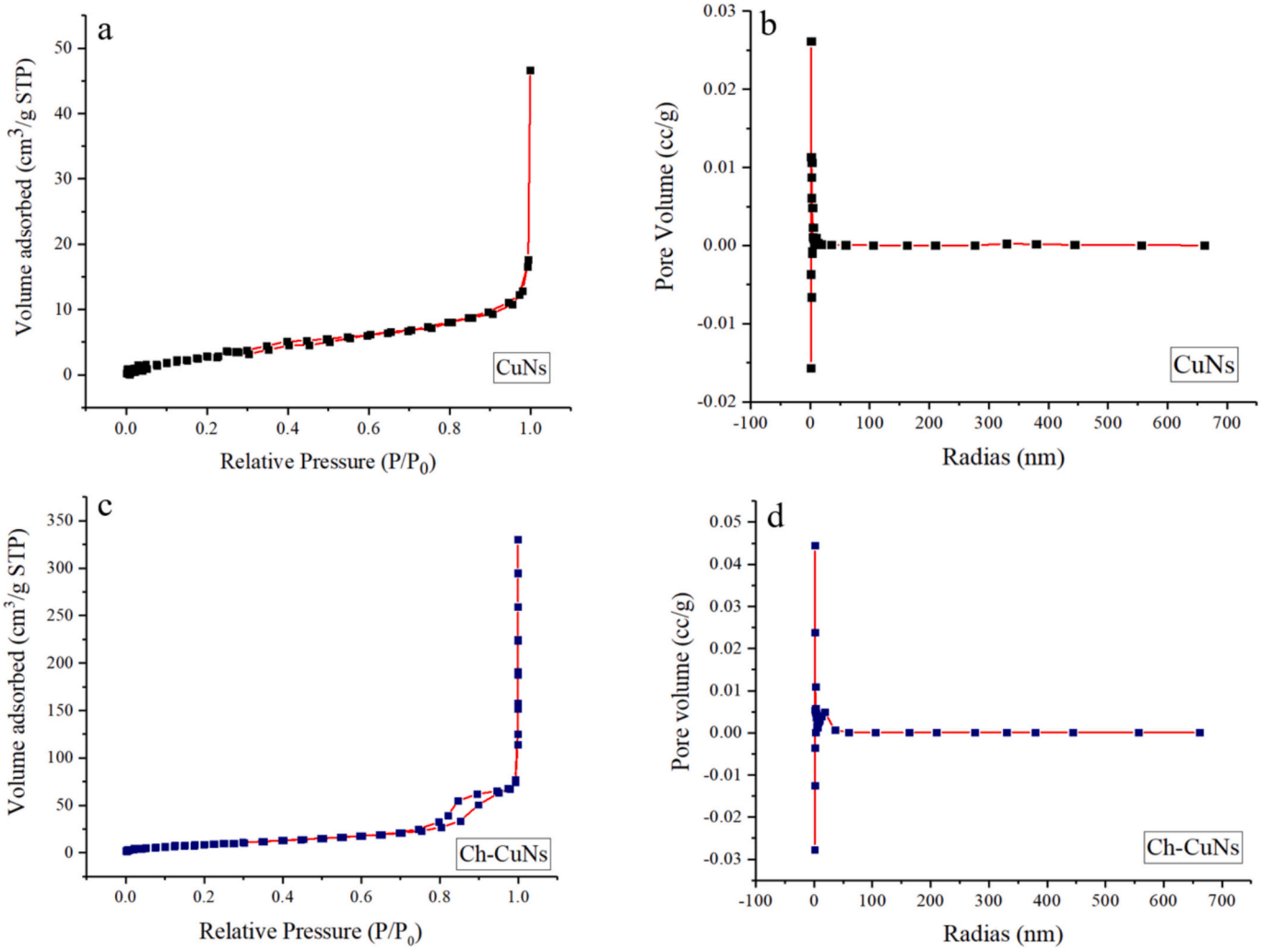

Fig. 6. Specific surface area CuNs (a) and Ch-CuNS (c). Porosity of CuNs (b) and Ch-CuNs (d).

amorphous area relatively increased. This is because the process synthesis of CuNs and Ch-CuNs nanocomposite produces highly amorphous CuNs and Ch-CuNs nanoparticles. Jia et al. [46] investigated XRD analysis of chitosan and reported a similar kind of result.

3.2. Biotransformation of Cr (VI) and proposed mechanism

Here, XPS was used to confirm the Cr (VI) reduction to Cr(III) at the surface of Ch-CuNs. The binding of Cr (VI) to the Ch-CuNs surface can be confirmed by the XPS spectra, which displayed peaks at the range of 566.08–592.58 eV. As indicated in Fig. 8, the decrease in the concentration of Cr (VI) on Ch-CuNs is correlated to the reduction of Cr(VI).

The conversion of Cr (VI) was demonstrated by the XPS signal of Cr2p3/2. Two oxidation states of chromium appear in Cr2p3/2 at binding energies of 592.587 and 566.086 eV, respectively. The major peak for Cr (III) was at 573.3–566.08 eV, while the minor snow peak for Cr (VI) was at 578.7–575 eV. The strong peak here is an indication of Cr (VI) changing to Cr (III). This conversion process is aligned with redox reactions as evidenced by Bandara et al. [47] employed a polymer based on graphene oxide adsorbent for the Cr (VI) reduction.

XPS analysis demonstrated that the Cr (VI) species on the surface of Ch-CuNs are reduced to Cr (III). On the other hand, FTIR spectroscopy revealed the participation of surface functional groups in the adsorption process of Cr (VI). The reduction mechanism of Cr (VI) can be elucidated using the data of these analyses and chemical reactions in order to elucidate the reduction mechanism. As long as the pH of the solution remains below 6.5, the metal can be found in the form of $HCrO_4^{2-}$ and $Cr_2O_7^{2-}$. Upon mixing dichromate ($Cr_2O_7^{2-}$) ions into water, they ionize and release chromate (CrO_4^{2-}) ions into the water. The conversion of $Cr_2O_7^{2-}$ in the water is shown in the Eq. (4).

$$Cr_2O_7^{2-} + H_2O \rightleftharpoons 2CrO_4^{2-} + 2H^+ \quad (4)$$

At acidic pH (pH 2–6), $HCrO_4^-$ ion species are the dominant form. The chemical reaction of CrO_4^{2-} conversion into $HCrO_4^-$ is shown in Eq. 5.

$$CrO_4^{2-} + H^+ \rightleftharpoons HCrO_4^- \quad (5)$$

Whenever the pH is acidic, chitosan's amine groups are positively charged. Chitosan's amines, hydroxyl groups, and alcoholic groups interact with chromium ion species. An anionic proton can bind with a negatively charged hydroxyl and amine group on chitosan [48]. An example of Cr (VI) binding to functional groups of chitosan is shown in Fig. 9.

Based on the redox potential of $HCrO_4^-$ (+1.34), it shows that it is strongly reducible and that the reduction reaction occurs following Eq. 6.

$$HCrO_4^- + 7H^+ + 3e^- \rightleftharpoons Cr^{3+} + 4H_2O \quad (6)$$

In acidic environments, Cr (VI) ions frequently interact with protonated groups on chitosan. These protonated groups can donate electrons to Cr (VI), facilitating its reduction to Cr (III), as observed by

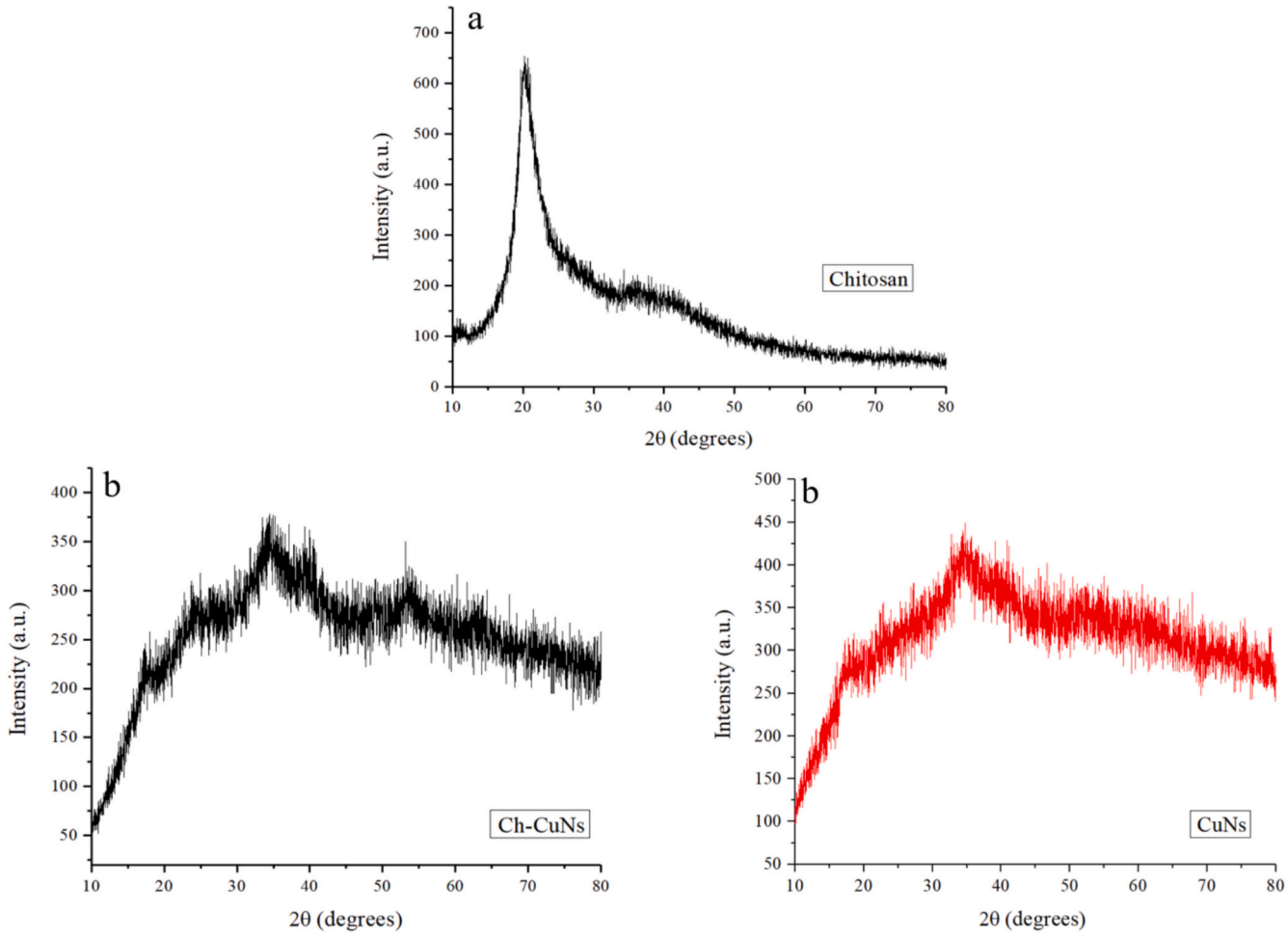

Fig. 7. XRD pattern of chitosan (a), CuNs (b) and Ch-CuNs.

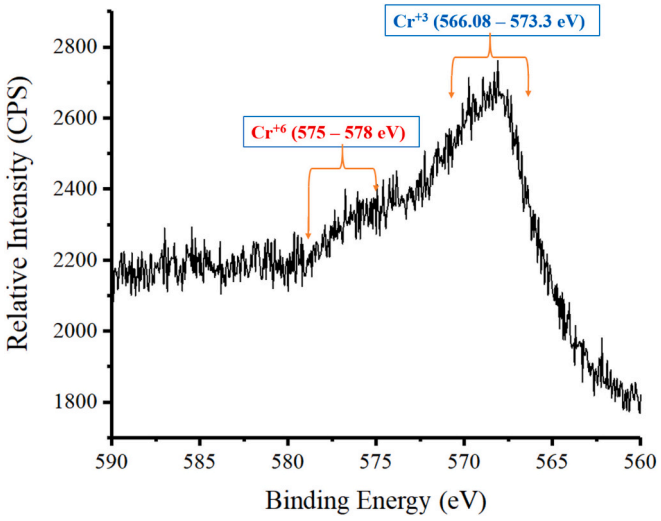

Fig. 8. Reduction of Cr (VI) into Cr (III) on Ch-CuNs.

Besharat et al. [49]. Ganglo et al. [50] reported the Cr (III) ions form a complex with the functional groups of chitosan. Indeed, Cr (III) is less soluble in water and has less chemical reactivity than Cr (VI), which can greatly affect chromium adsorption [47]. The Cr (III) ions are still anchored on the Ch-CuNs surface via chelation and ligand exchange interactions. Previous studies have shown that chitosan-coated surfaces are very effective in adsorbing and biotransforming Cr (VI) to Cr (III), such as the use of chitosan coating on ceramic alumina and chitosan-coated cotton fibers [51,52].

3.3. Cr (VI) adsorption

The effect of various parameters such as pH, temperature, initial Cr (VI) concentration, Ch-CuNs dosages, contact time and agitation rate are mentioned in the section S5 of supplementary data [53–60].

3.3.1. Kinetic modeling

Kinetic models help determine the mechanism of Cr (VI) adsorption on Ch-CuNs. Pseudo-first-order, pseudo-second-order and Elovich kinetics were investigated and represented in Fig. 10.

The kinetic parameters were calculated from the graphs of adsorption data and represented in Table 1.

Higher R^2 and lower residual sum of squares (RSS) indicate that the pseudo-second-order model best fits in the adsorption data as compared to pseudo-first-order and Elovich models. This indicates that the main process of adsorption mechanism involved was chemisorption. A low value of *h* suggests that the adsorption of Cr (VI) onto the adsorbent was fast at the beginning and decreased with the progression of time. Ayoub et al. [61] have reported similar findings. Authors reported that Cr (VI) adsorption onto pine needle-activated carbon conformed to a pseudo-second-order kinetic model, suggesting that the rate limiting step is chemisorption. Additionally, Wang et al. [27] observed that the adsorption of Cr (VI) onto Fe_3O_4 nanoparticle-covered mushrooms followed the pseudo-second-order model.

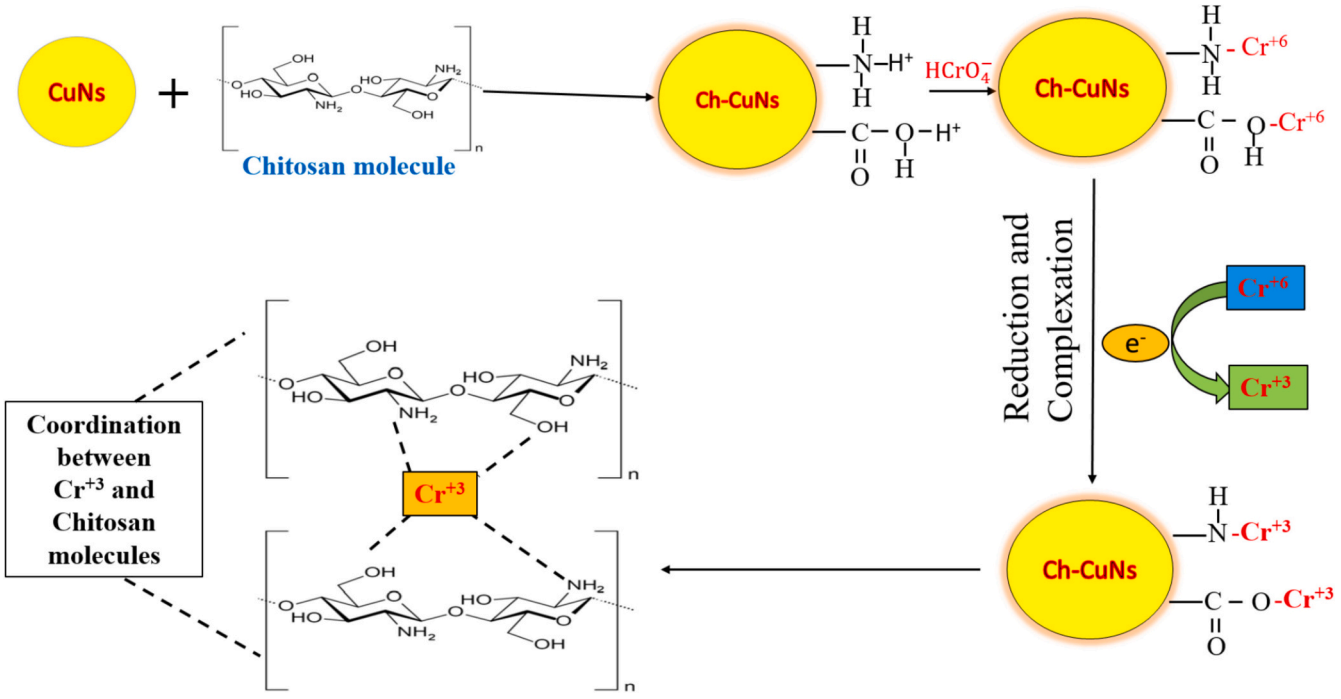

Fig. 9. Proposed mechanism of Cr (VI) removal by Ch-CuNs.

3.3.2. *Isotherm study*

Isotherm studies were conducted using Langmuir, Freundlich, Temkin, and Halsey models to analyze adsorption data (Fig. 11).

These models provide useful information on the adsorption mechanism, surface characteristics, and adsorbate-adsorbent interactions. The Langmuir adsorption isotherm assumes monolayer adsorption onto a surface with a limited number of identical sites. On the other hand, the Freundlich model is often used to describe adsorption on heterogeneous surfaces, where adsorption occurs in multiple layers, and different sites have different energies of adsorption. The work of Temkin regarding indirect adsorbate-adsorbate interactions and Halsey for multilayer adsorption. Experimental data was utilized to calculate the parameters and constant of isotherm models which were mentioned in Table 2.

Based on the higher R^2 (0.99) and lower RSS value, it can be confirmed that the Freundlich model is suitable for describing the adsorption of Cr (VI) onto Ch-CuNs. This indicates that multilayer formation occurs during the adsorption process and the surface of heterogeneity. Finally, the constant 'b_T' of the Temkin model suggested that the adsorption process was endothermic, which was consistent with the thermodynamic results of this study. Emamy et al. [62] investigated that 'n_H' value from Halsey isotherm also shows that there is a positive cooperativity between Cr (VI) ions and Ch-CuNs at the temperature of 20, 25 and 50 °C. This is in line with similar findings by Singh et al. [63] reported a better fit of the Freundlich isotherm for Cr (VI) adsorption by using chitosan-coated MnO_2 nanoparticles. Zheng et al. [64] also found the Freundlich isotherm fit the Cr (VI) adsorption on 4-vinyl pyridine modified magnetic chitosan biopolymer and chitosan-based hydrogel, respectively. The similar values of b obtained in other studies also suggest the applicability of the Freundlich model in characterizing Cr (VI) adsorption processes, which is highly related to the heterogeneous and multilayer nature of the adsorption mechanism.

3.3.3. *Thermodynamic study*

The adsorption of Cr (VI) was performed at different temperature ranges from 20 to 50 °C and represented in Fig. 12.

The thermodynamic parameters were calculated from the graph (Fig. 12) and shown in Table 3.

The positive enthalpy change (ΔH°) for Cr (VI) adsorption indicates that the process is endothermic, requiring heat absorption from the surroundings. This endothermic nature typically enhances adsorption capacity with increasing temperature, as the adsorbent's affinity for the heavy metal increases. Such behaviour is characteristic of chemisorption processes, where bond formation occurs between the adsorbate and adsorbent, as investigated by Egbosiuba et al. [65]. A positive entropy change (ΔS°) of 60.09 J K^{-1} mol^{-1} suggests that the adsorption is favourable, accompanied by increased randomness at the solid-liquid interface. The negative Gibbs free energy (ΔG°) values at temperatures of 20, 35, and 50 °C indicate that the adsorption is spontaneous, with spontaneity increasing as temperature rises, highlighting a strong temperature dependence of Cr (VI) adsorption. Similar findings were reported by Fang et al. [66] for Cr (VI) adsorption using zero-valent iron-based materials. Zhu et al. [67] observed the endothermic nature of Cr (VI) adsorption onto nanoscale zero-valent iron/nickel composites.

4. Comparison of adsorption capacity

The adsorption capacity of Ch-CuNs is compared with other nanomaterials in Table 4.

Among the various nano-adsorbents compared, Ch-CuNs exhibit a high adsorption capacity (91.96 mg/g) with an optimal pH of 2 and a moderate contact time of 300 min. Although PEI-silica nanoparticles show a higher capacity (183.70 mg/g), they require an excessively long contact time of 1440 min, making them less practical for real-time applications [69]. Similarly, while some materials like industrial fly ash-magnetite (96.37 mg/g) and chitosan-grafted graphene oxide (104.16 mg/g) demonstrate competitive capacities, their performance under comparable initial Cr (VI) concentrations and higher contact durations does not outperform Ch-CuNs [72,78]. Importantly, Ch-CuNs follow pseudo-second-order kinetics, indicating efficient and chemisorptive interaction with Cr(VI) ions. Furthermore, many other adsorbents such as GO (1.2×10^{-3} mg/g) and $MnFe_2O_4$ (34.84 mg/g) show significantly lower capacities [71,74]. Thus, Ch-CuNs offer an ideal balance between high adsorption performance, appropriate contact time, and effective kinetics, making them a suitable candidate for Cr(VI) removal in contaminated water.

The removal efficiency of synthesized Ch-CuNs were tested in a

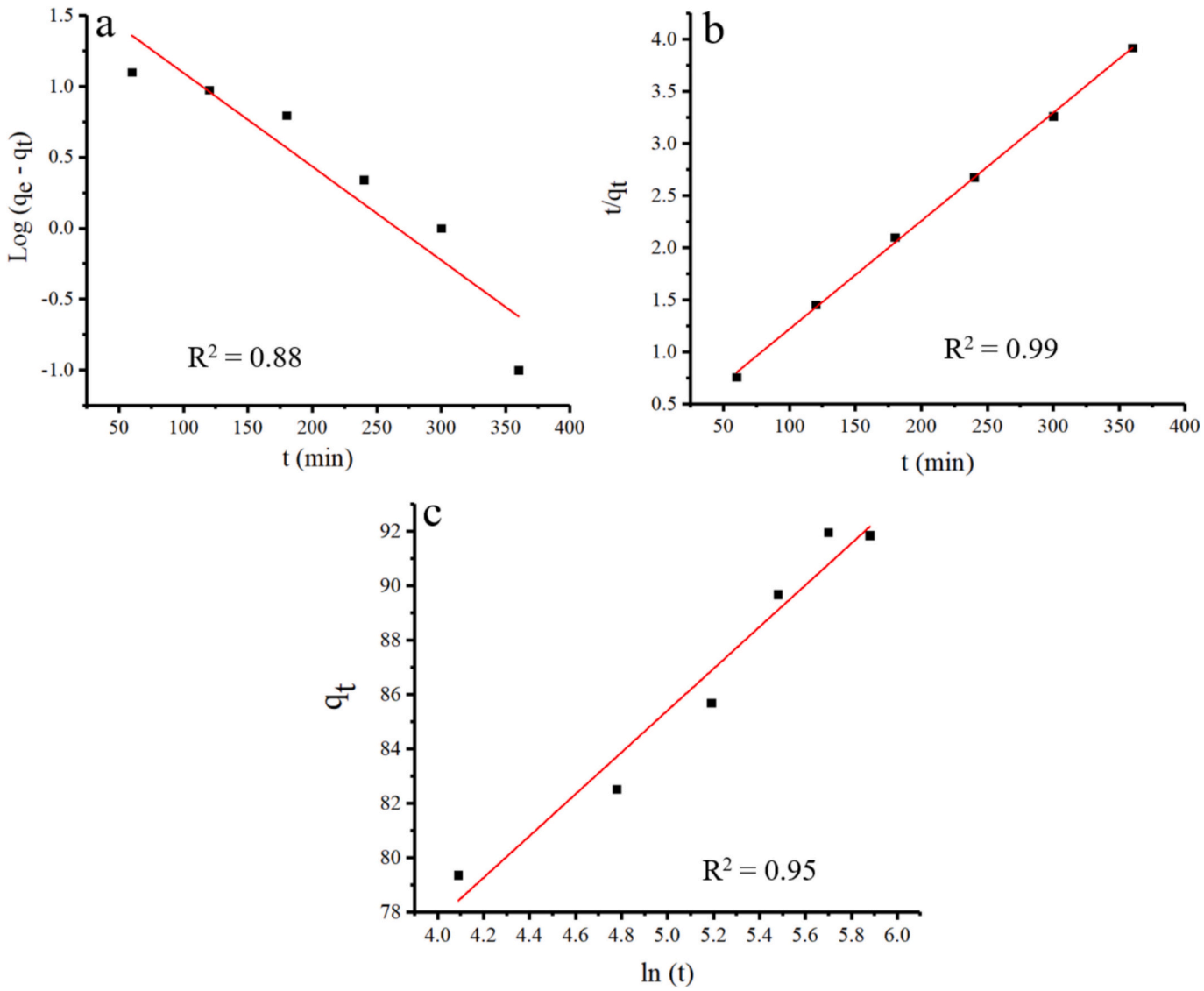

Fig. 10. Pseudo-first-order (a), pseudo-second-order (b) and Elovich (c) kinetics of Cr (VI) adsorption.

Table 1
Kinetics parameter for Cr (VI) adsorption.

Pseudo-first order				Pseudo-second order				Elovich kinetic			
k_s (min^{-1})	q_e (mg/g)	R^2	RSS	k'_2 (mg/g min^{-1})	h (mg/g min^{-1})	R^2	RSS	α (μg g^{-1} min^{-1})	β (g $μg^{-1}$)	R^2	RSS
−0.006	1.75	0.88	0.34	0.179	0.01	0.99	0.0067	7.68	46.97	0.95	5.50

simultaneous system containing competing ions Cd(II), Pb(II), As(III), and Ni(II). Ch-CuNs achieved removal efficiencies of 89.86 % for Cr(VI), 85.45 % for Cd(II), 75.87 % for Pb(II), 79.28 % for As(III), and 71.95 % for Ni(II), demonstrating effective multi-ion removal capability and confirming their potential for treating contaminated water with complex heavy metal mixtures.

5. Desorption of Cr (VI) and regeneration of adsorbent

An adsorbent's practicality and viability are enhanced when it can be reused across multiple adsorption and desorption cycles. In this study, Ch-CuNs were successfully regenerated using 0.1 N nitric acid (HNO_3) as the eluent. The effectiveness of these cycles is illustrated in Fig. 13, which shows the adsorption and desorption processes over multiple cycles.

Specific studies focussing upon the Cr (VI) adsorption-desorption behaviour onto Ch-CuNs provide new important insights related to the material's reusability and stability. As shown in Fig. 13, the adsorption efficiency of Ch-CuNs dropped from 91.96 % to 69.76 % in the first five cyclic runs due to the difficulty in maintaining performance during multiple uses. This decrease is ascribed to cumulative structural and chemical modifications of the adsorbent. Some of the weight lost during washing and elution processes was probably due to physical loss, which reduced the available surface area for subsequent phases of adsorption [81]. Simultaneously, the active sites, particularly protonated amino ($-NH_3^+$) and hydroxyl (−OH) groups on chitosan, became inactivated due to an irreversible crosslinking with Cr (VI) oxyanions, e.g., $HCrO_4^-$, CrO_4^{2-} [81]. Even using strong desorption agents such as HCl or NaOH,

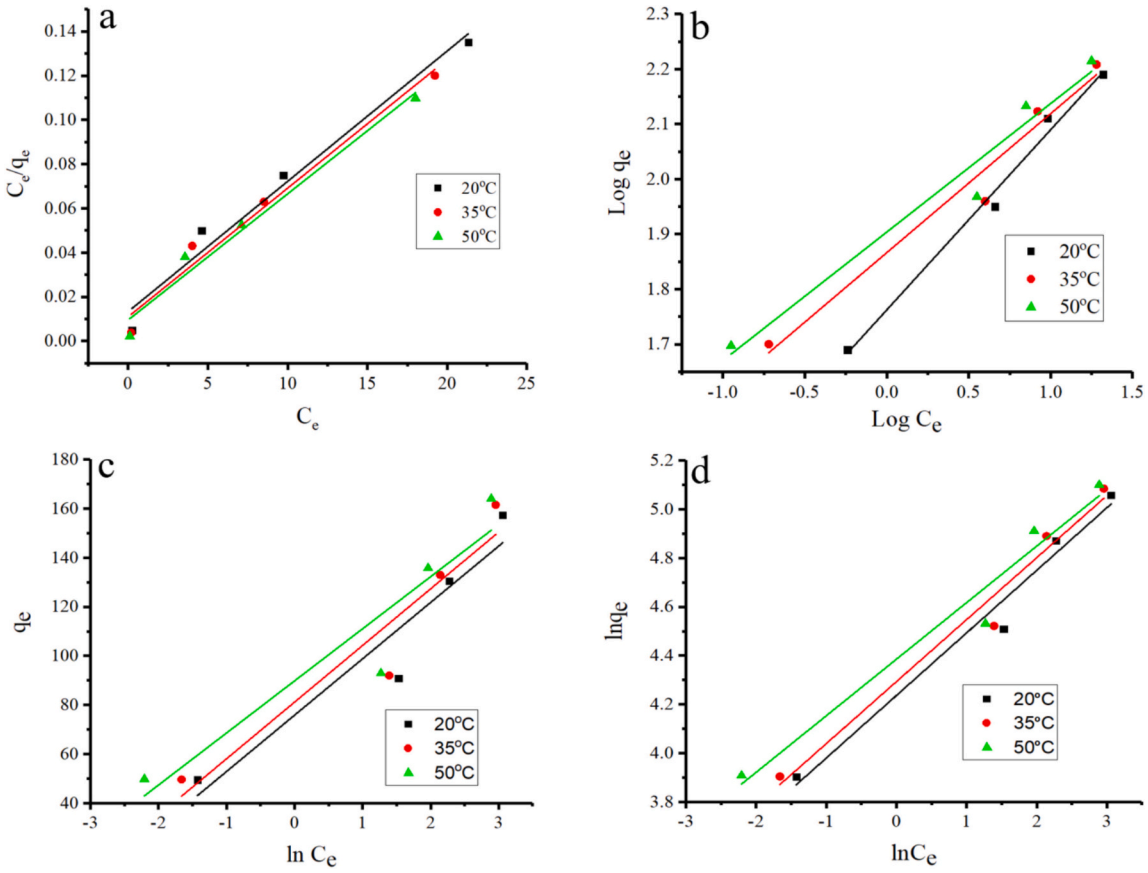

Fig. 11. Langmuir (a), Freundlich (b), Temkin (c) and Halsey (d) isotherm study of Cr (VI) adsorption.

Table 2
Isotherms parameters.

Isotherms	Parameters	20 °C	35 °C	50 °C
Langmuir	B	0.013	0.011	0.009
	Q^0	0.0059	0.0058	0.0057
	R^2	0.97	0.97	0.97
	RSS	2.23	1.57	1.41
Freundlich	k_f	1.76	1.86	1.90
	N	0.32	0.25	0.23
	R^2	0.98	0.99	0.99
	RSS	0.0015	0.0045	0.0056
Temkin	A_T	75.84	81.15	89.81
	b_T	22.96	23.08	21.22
	R^2	0.91	0.90	0.89
	RSS	580.58	653.53	799.90
Halsey	K_H	0.26	0.25	0.23
	n_H	4.23	4.29	4.38
	R^2	0.97	0.97	0.96
	RSS	0.019	0.021	0.030

which attained desorption efficiencies of 85.91–52.23 %, regeneration was still not completed. Strong chemisorption mechanisms, comprising electrostatic attraction, surface complexation, or partial reduction of Cr (VI) to Cr (III) stabilize a fraction of the residual Cr (VI) ions retained on Ch-CuNs [82].

A comparative study on magnetic chitosan composites exhibited a 30 % decline in adsorption efficiency after five cycles due to pore collapse and active site saturation. The interplay between adsorbent morphology and Cr (VI) speciation under varying pH conditions further complicates regeneration. At low pH, the dominance of $HCrO_4^-$ enhances electrostatic binding to protonated Ch-CuNs, but subsequent elution at alkaline pH weakens these interactions incompletely, leaving residual complexes [83].

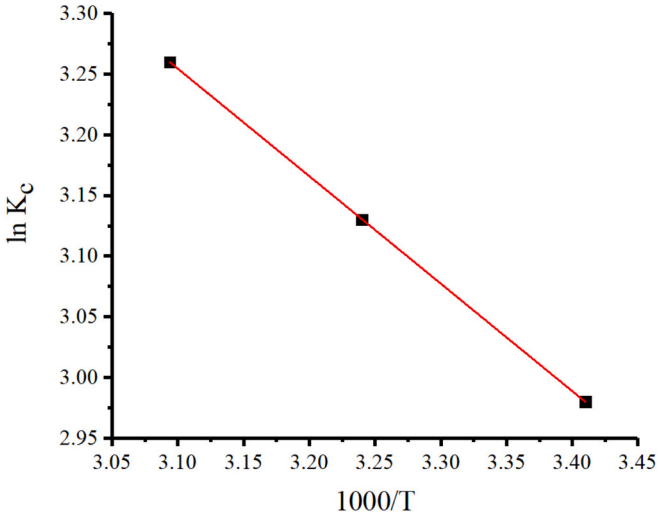

Fig. 12. Thermodynamic study of Cr (VI) adsorption.

Table 3
Thermodynamic data for adsorption of Cr (VI) onto Ch-CuNs.

T (°C)	ΔG° (J mol^{-1})	ΔH° (J mol^{-1})	ΔS° (J K^{-1} mol^{-1})
20	−7263.00		
35	−8018.93	885.97	60.09
50	−8758.54		

Based on the data collected across multiple adsorption and

Table 4
Comparison of adsorption capacity of Ch-CuNs with other nanoparticles.

Adsorbents	Adsorption Capacity (mg/g)	Optimum pH	Contact Time (min)	Kinetics	Initial Cr (VI) concentration	Reference
Chitosan-Coated Iron Oxide Nanocomposite Membranes	14.45	4	30	Pseudo second order	25	[68]
PEI-silica nanoparticle	183.70	2	1440	–	10–200	[69]
Magnetite–diatomite nanocomposite	88.49	3	30	Pseudo second order	16	[70]
Nano-magnetic $MnFe_2O_4$	34.84	2	10	Pseudo second order	55	[71]
Industrial waste (fly ash)-magnetite particles	96.37	4.5	120	Pseudo second order	28.5	[72]
Nanometer zero-valent iron on modified activated carbon	66.00	2	180	Pseudo second order	100	[73]
Graphene oxide (GO) from graphite	1.2×10^{-3}	4	40	Pseudo second order	–	[74]
Nanoscale ZVI + Chitosan-functionalized *Eichhornia crassipes* biochar	82.20	2	–	Pseudo second order	50	[75]
Amino-functionalized carbon nanospheres	52.38	3	60	–	50	[76]
Polyaniline-coated microcrystalline cellulose nanocomposites	35.97	7	120	Pseudo second order	10	[77]
Chitosan-grafted graphene oxide nanocomposite	104.16	2	420	Pseudo second order	50	[78]
AgNPs/GO/chitosan nanocomposite	44.00	4	80	Pseudo second order	50	[79]
Nanoscale ZVI-biochar-alginate composite	86.40	4	–	Pseudo second order	150	[80]
Chitosan-Coated Copper Nanoparticles (Ch-CuNs)	91.96	2	300	Pseudo second order	50	*Present study*

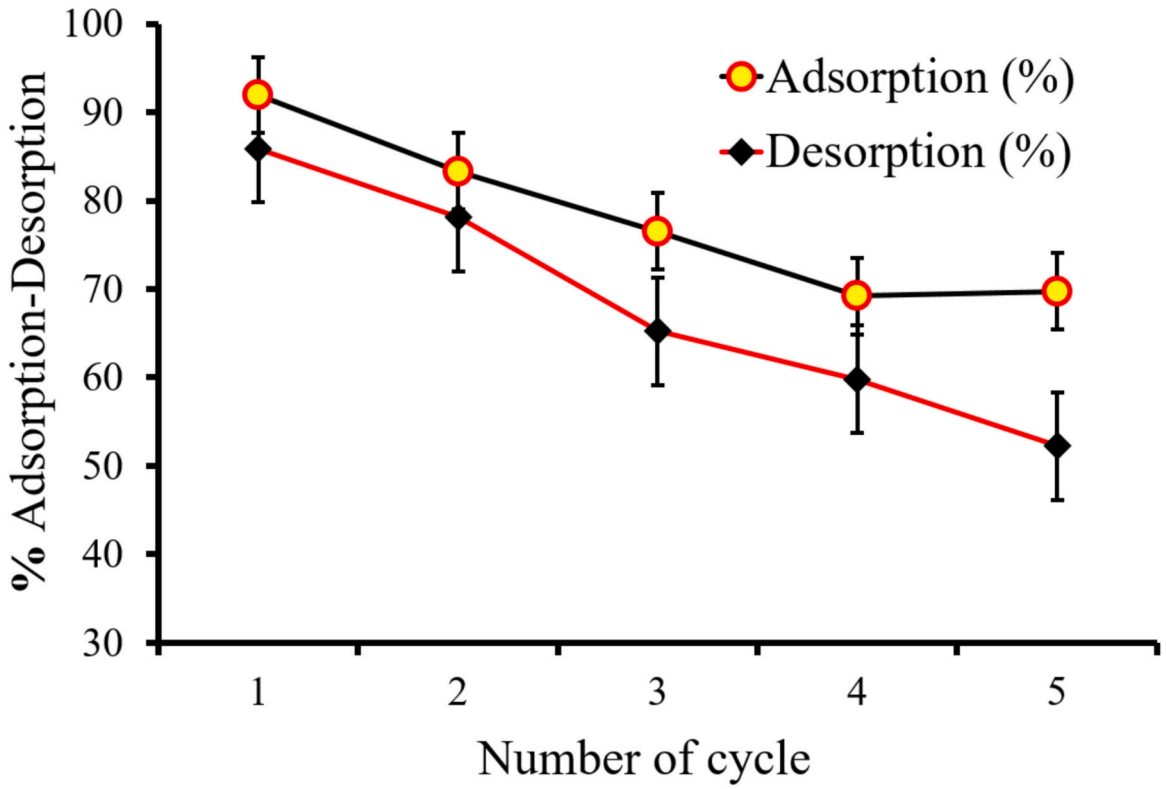

Fig. 13. Adsorption-desorption study of Cr (VI) by Ch-CuNs.

desorption cycles, repeated measures analysis of variance (RM-ANOVA) was performed to evaluate whether the differences in Cr (VI) adsorption and desorption across multiple regeneration cycles were statistically significant. Since the same adsorbent material (Ch-CuNs) was used across all cycles, RM-ANOVA was appropriate to account for the within-sample dependency. The following Table 5 presents the results of the analysis for both adsorption and desorption (Table 5).

Repeated measures ANOVA revealed statistically significant differences in both Cr (VI) Adsorption and Desorption across cycles as ($p < 0.001$). This indicates that regeneration cycles had a strong influence on the adsorption and desorption for Cr (VI).

Table 5
Repeated measures ANOVA results for Cr (VI) adsorption and desorption across regeneration cycles.

Variables	Sources of variation	Degrees of freedom	Sum of squares	Mean sum of squares	F- Test value	p-value
Adsorption	Between Groups	4	1109.25	277.31		
	Between Subjects	2	34.61	17.31	63.75	<0.001
	Error	8	34.81	4.35		
	Total	14	1178.67			
Desorption	Between Groups	4	2239.73	559.93		
	Between Subjects	2	7.73	3.87	166.65	<0.001
	Error	8	26.6	3.36		
	Total	14	2274.06			

6. Complete removal of Cr (VI) from contaminated water by series reactor system

Despite having a high capacity for absorption of Cr (VI) (91.96 mg/g), Ch-CuNs retain 8.04 mg/L of Cr (VI) in the liquid phase after removing 91.96 % of the Cr (VI) from an aqueous solution with an initial concentration of 50 mg/L in the first round. The amount of Cr (VI) that is still present in the water is significantly more than the allowable discharge limit. Therefore, the treated metal ion solution from the first reactor was recirculated into the second reactor, which was added in sequence, to remove the residual Cr (VI). After the second round of treatment, there is a 100 % elimination of Cr (VI), which satisfies the discharge guidelines. Fig. 14 displays the comprehensive experimental configuration.

7. Strengths and limitations

This study demonstrates a green, sustainable, and cost-effective approach for Cr (VI) remediation using Ch-CuNs. A major strength lies in the eco-friendly synthesis protocol, which avoids toxic reagents while utilizing waste resources. Comprehensive characterization through FTIR, SEM-EDX, BET, XRD, and XPS confirmed successful nanoparticle formation, functionalization, and Cr (VI) reduction. The study presents robust adsorption performance, achieving a high removal capacity, favourable thermodynamic parameters, and pseudo-second-order kinetic behaviour, indicating chemisorption. Statistical validation using ANOVA, Pearson correlation, and RM-ANOVA strengthens the reliability of experimental outcomes. This study also provides mechanistic insights into the Cr (VI) biotransformation into Cr (III), a less toxic form, enhancing its environmental relevance.

However, the study is limited to batch and series reactor systems, which may not fully simulate real-world wastewater conditions. Regeneration efficiency and potential secondary environmental impacts of the used nanomaterials require further exploration. Moreover, while chitosan coating improved surface area and adsorption efficiency, its long-term structural stability under variable environmental conditions remains to be validated through pilot-scale or field applications.

8. Conclusion

In this study, curcumin extract was combined with *citrus limetta* peel powder to synthesise Ch-CuNs. The HR-SEM analysis revealed that Ch-CuNs have a rough surface and a spherical shape. FTIR analysis revealed the presence of hydroxyl, carboxyl, and amino groups. EDX analysis confirmed the presence of Cu, O, C, H, and N. Cr (VI) was absorbed into Ch-CuNs and reduced to Cr (III). There was a better fit with the Freundlich isotherm ($R^2 = 0.99$) and a pseudo-second-order kinetic model for Cr (VI) on Ch-CuNs, indicating chemisorption. In desorption studies, Ch-CuNs were shown to be reusable multiple times with a high shelf life. Due to the higher adsorption capacity and eco-friendly nature of Ch-CuNs, it can be considered a suitable adsorbent for the removal of water contaminations including Cd (II), Pb (II), As (II), and organic contaminants. Life cycle assessment (LCA) and techno-economic analysis can be further applied to scale up the water treatment process.

CRediT authorship contribution statement

Veer Singh: Writing – review & editing, Writing – original draft, Visualization, Validation, Methodology, Investigation, Formal analysis, Data curation, Conceptualization. **Anurag Kumar Singh:** Writing – review & editing, Methodology, Conceptualization. **Kumar Abhishek:** Writing – review & editing, Validation. **Vikash Kumar:** Writing – review & editing, Formal analysis. **Ravi Ranjan:** Writing – review & editing, Validation. **Shobha Kumari:** Writing – review & editing. **Sonali Vedika:** Writing – review & editing, Formal analysis. **Ashiq Hussain Bhat:** Writing – review & editing, Formal analysis. **Vishal Mishra:** Writing – review & editing, Investigation. **Ashish Kumar:** Writing – review & editing, Supervision, Investigation, Formal analysis, Conceptualization.

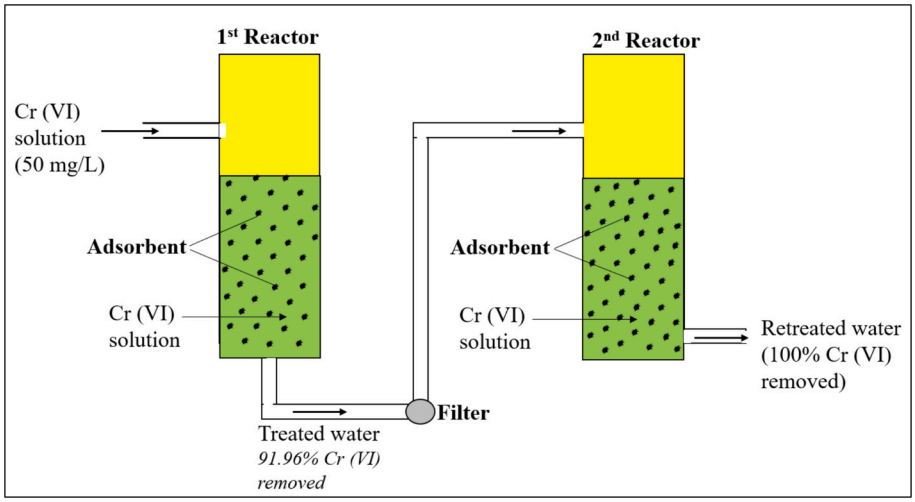

Fig. 14. Diagrammatic representation of Cr (VI) removal in the series reactor system.

Funding

This research did not receive any specific grant from funding agencies in the public, commercial, or not-for-profit sectors.

Declaration of competing interest

The authors declare that they have no known competing financial interests or personal relationships that could have appeared to influence the work reported in this paper.

Acknowledgements

The authors of this manuscript are thankful to the RMRIMS, Patna, India for providing the necessary support during this study. Dr. Veer Singh thanks the Department of Health Research, India (DHR) and Indian Council of Medical Research (ICMR) for granting the Young Scientist Award (File No.R.12014/37/2022-HR). We are also thankful to Miss Surya Suman and Mr. Dheeren Kumar for providing technical assistance.

Appendix A. Supplementary data

Supplementary data to this article can be found online at https://doi.org/10.1016/j.ijbiomac.2025.146868.

Data availability

No data was used for the research described in the article.

References

[1] J.P. Wise, J.L. Young, J. Cai, L. Cai, Current understanding of hexavalent chromium [Cr(VI)] neurotoxicity and new perspectives, Environ. Int. 158 (2021) 106877, https://doi.org/10.1016/j.envint.2021.106877.
[2] M. Tumolo, V. Ancona, D. De Paola, D. Losacco, C. Campanale, C. Massarelli, V. F. Uricchio, Chromium pollution in European water, sources, health risk, and remediation strategies: an overview, Int. J. Environ. Res. Public Health 17 (2020) 5438, https://doi.org/10.3390/ijerph17155438.
[3] R. Vengosh, J. Coyte, J.S. Karr, A.J. Harkness, L.S. Kondash, R.B. Ruhl, G.S. Merola, Dywer, Origin of hexavalent chromium in drinking water wells from the Piedmont aquifers of North Carolina, Environ. Sci. Technol. Lett. 3 (2016) 409–414, https://doi.org/10.1021/acs.estlett.6b00342.
[4] Ş. Akkurt, M. Oğuz, A.A. Uçkun, Bioreduction and bioremoval of hexavalent chromium by genetically engineered strains (*Escherichia coli* MT2A and *Escherichia coli* MT3), World J. Microbiol. Biotechnol. 38 (2022), https://doi.org/10.1007/s11274-022-03235-2.
[5] World Health Organization, Guidelines for Drinking-Water Quality, 4th ed., WHO, Geneva, Switzerland, 2011. https://www.who.int/publications/i/item/9789241549950. (Accessed 24 April 2017).
[6] United States Environmental Protection Agency. Chromium (VI) in Drinking Water, EPA, Washington, DC, 2020. https://www.epa.gov/sdwa/chromium-drinking-water (accessed 5 August 2025).
[7] A. Saravanan, P.S. Kumar, S. Varjani, S. Karishma, S. Jeevanantham, P. R. Yaashikaa, Effective removal of Cr(VI) ions from synthetic solution using mixed biomasses: kinetic, equilibrium and thermodynamic study, J Water Process Eng 40 (2021) 101905, https://doi.org/10.1016/j.jwpe.2020.101905.
[8] H. Kaur, N. Devi, S.S. Siwal, W.F. Alsanie, M.K. Thakur, V.K. Thakur, Metal–organic framework-based materials for wastewater treatment: superior adsorbent materials for the removal of hazardous pollutants, ACS Omega 8 (2023) 9004–9030, https://doi.org/10.1021/acsomega.2c07719.
[9] P. Thamarai, R. Kamalesh, A. Saravanan, P. Swaminaathan, V.C. Deivayanai, Emerging trends and promising prospects in nanotechnology for improved remediation of wastewater contaminants: present and future outlooks, Environ. Nanotechnol. Monit. Manage. 21 (2024) 100913, https://doi.org/10.1016/j.enmm.2024.100913.
[10] J. Ye, Y. Wang, Q. Xu, H. Wu, J. Tong, J. Shi, Removal of hexavalent chromium from wastewater by cu/Fe bimetallic nanoparticles, Sci. Rep. 11 (2021), https://doi.org/10.1038/s41598-021-90414-0.
[11] M.C. Crisan, M. Teodora, M. Lucian, Copper nanoparticles: synthesis and characterization, physiology, toxicity and antimicrobial applications, Appl. Sci. 12 (2021) 141, https://doi.org/10.3390/app12010141.
[12] A. Antonio-Pérez, L.F. Durán-Armenta, M.G. Pérez-Loredo, A.L. Torres-Huerta, Biosynthesis of copper nanoparticles with medicinal plants extracts: from extraction methods to applications, Micromachines 14 (2023) 1882, https://doi.org/10.3390/mi14101882.
[13] M. Tefera, R. Fekadu, F.F. Eshete, D.M. Kabtamu, M. Gashu, A. Tadesse, N. Belachew, Visible-light-driven reduction of chromium (VI) by green synthesised cuprous oxide nanoparticles, J. Mol. Liq. 359 (2022) 119272, https://doi.org/10.1016/j.molliq.2022.119272.
[14] N.V. Noory, N.R. Saeedy, Green synthesis of copper oxide nanoparticles using *Citrus limetta* (sweet lime) peel waste, Magna Sci. Adv. Biol. Pharm. 2 (2021) 010–013, https://doi.org/10.30574/msabp.2021.2.2.0020.
[15] G.E. Putri, A. Labanni, S. Arief, P. Dafriani, I.Y. Darma, S. Handayani, N. Widyastuti, N. Jaffar, M. Mahmud, A.H. Ritonga, Green synthesis of cerium oxide nanoparticles using Citrus nobilis Lour. Peel extract and evaluation of their potential as antibacterial and antioxidant agents, case stud, Chem. Environ. Eng. (2024) 101062, https://doi.org/10.1016/j.cscee.2024.101062.
[16] F. Hisham, M.H.M. Akmal, F. Ahmad, K. Ahmad, N. Samat, Biopolymer chitosan: potential sources, extraction methods, and emerging applications, Ain Shams Eng. J. 15 (2023) 102424, https://doi.org/10.1016/j.asej.2023.102424.
[17] A. Reda, A.-G. El-Demerdash, W. Sadik, E. El-Rafey, T. Shoeib, Effectively eliminating lead and cadmium from industrial wastewater using a biowaste-based sorbent, Appl Water Sci 15 (2025), https://doi.org/10.1007/s13201-024-02343-8.
[18] A.R. Aly, A.-G. El-Demerdash, W. Sadik, E.E. Rafy, T. Shoeib, Upcycling of sugar refining mud solid waste as a novel adsorbent for removing methylene blue and Congo red from wastewater, RSC Adv. 14 (2024) 13505–13520, https://doi.org/10.1039/d4ra01451k.
[19] H. Yazid, T. Bouzid, E.M.E. Mouchtari, L. Bahsis, M.E. Himri, S. Rafqah, M. E. Haddad, Insights into the adsorption of Cr(VI) on activated carbon prepared from walnut shells: combining response surface methodology with computational calculation, Clean Technol. 6 (2024) 199–220, https://doi.org/10.3390/cleantechnol6010012.
[20] Y. Zhou, Y. Zhao, X. Wu, W. Yin, J. Hou, S. Wang, K. Feng, X. Wang, Adsorption and reduction of hexavalent chromium on magnetic greigite (Fe3S4)-CTAB: leading role of Fe(ii) and S(−ii), RSC Adv. 8 (2018) 31568–31574, https://doi.org/10.1039/c8ra06534a.
[21] O. Tobbi, Z. Hattab, H. Boutefnouchet, B. Benouis, F. Benamia, R. Djellabi, Cost-effective walnut shell biosorbent for efficient Cr(VI) removal from water: batch adsorption and optimization using RSM-BBD, Desalin. Water Treat. (2024) 100783, https://doi.org/10.1016/j.dwt.2024.100783.
[22] S. Kanwal, P. Devi, Z. Ahmed, N.A. Qambrani, Adsorption isotherm, kinetic and thermodynamic studies for adsorption of fluoride on waste marble powder, Desalin. Water Treat. 319 (2024) 100441, https://doi.org/10.1016/j.dwt.2024.100441.
[23] D. Ewis, M.M. Ba-Abbad, A. Benamor, N. Mahmud, M. Nasser, M. El-Naas, A. W. Mohammad, Adsorption of 4-Nitrophenol onto Iron oxide bentonite nanocomposite: process optimization, kinetics, isotherms and mechanism, Int. J. Environ. Res. 16 (2022), https://doi.org/10.1007/s41742-022-00402-z.
[24] S. Raghav, D. Kumar, Comparative kinetics and thermodynamic studies of fluoride adsorption by two novel synthesized biopolymer composites, Carbohydr. Polym. 203 (2018) 430–440, https://doi.org/10.1016/j.carbpol.2018.09.054.
[25] U.A. Edet, A.O. Ifelebuegu, Kinetics, isotherms, and thermodynamic modeling of the adsorption of phosphates from model wastewater using recycled brick waste, Processes 8 (2020) 665, https://doi.org/10.3390/pr8060665.
[26] S. Suresh, S. Karthikeyan, K. Jayamoorthy, FTIR and multivariate analysis to study the effect of bulk and nano copper oxide on peanut plant leaves, J. Sci. Adv. Mater. Devices 1 (2016) 343–350, https://doi.org/10.1016/j.jsamd.2016.08.004.
[27] C. Wang, H. Liu, Z. Liu, Y. Gao, B. Wu, H. Xu, Fe 3 O 4 nanoparticle-coated mushroom source biomaterial for Cr(VI) polluted liquid treatment and mechanism research, R. Soc. Open Sci. 5 (2018) 171776, https://doi.org/10.1098/rsos.171776.
[28] C. Quintelas, R. Pereira, E. Kaplan, T. Tavares, Removal of Ni(II) from aqueous solutions by an Arthrobacter viscosus biofilm supported on zeolite: from laboratory to pilot scale, Bioresour. Technol. 142 (2013) 368–374, https://doi.org/10.1016/j.biortech.2013.05.059.
[29] C.-L. Feng, J. Li, X. Li, K.-L. Li, K. Luo, X.-S. Liao, T. Liu, Characterization and mechanism of lead and zinc biosorption by growing Verticillium insectorum J3, PLoS One 13 (2018) e0203859, https://doi.org/10.1371/journal.pone.0203859.
[30] Y. Jin, S. Yu, C. Teng, T. Song, L. Dong, J. Liang, X. Bai, X. Xu, J. Qu, Biosorption characteristic of Alcaligenes sp. BAPb.1 for removal of lead(II) from aqueous solution, 3 Biotech 7 (2017), https://doi.org/10.1007/s13205-017-0721-x.
[31] R. Saha, K. Mukherjee, I. Saha, A. Ghosh, S.K. Ghosh, B. Saha, Removal of hexavalent chromium from water by adsorption on mosambi (*Citrus limetta*) peel, Res. Chem. Intermed. 39 (2012) 2245–2257, https://doi.org/10.1007/s11164-012-0754-z.
[32] L. Al-Naamani, J. Dutta, S. Dobretsov, Nanocomposite zinc oxide-chitosan coatings on polyethylene films for extending storage life of okra (*Abelmoschus esculentus*), Nanomaterials 8 (2018) 479, https://doi.org/10.3390/nano8070479.
[33] A. Buccolieri, A. Serra, G. Maruccio, A.G. Monteduro, S.K. Padmanabhan, A. Licciulli, V. Bonfrate, L. Salvatore, D. Manno, L. Calcagnile, G. Giancane, Synthesis and characterization of mixed Iron-manganese oxide nanoparticles and their application for efficient nickel ion removal from aqueous samples, J. Anal. Methods Chem. 2017 (2017) 1–9, https://doi.org/10.1155/2017/9476065.
[34] P. Hu, J. Wang, R. Huang, Simultaneous removal of Cr(VI) and Amido black 10B (AB10B) from aqueous solutions using quaternized chitosan coated bentonite, Int. J. Biol. Macromol. 92 (2016) 694–701, https://doi.org/10.1016/j.ijbiomac.2016.07.085.
[35] K.D. Khalil, S.M. Riyadh, S.M. Gomha, I. Ali, Synthesis, characterization and application of copper oxide chitosan nanocomposite for green regioselective synthesis of [1,2,3] triazoles, Int. J. Biol. Macromol. 130 (2019) 928–937, https://doi.org/10.1016/j.ijbiomac.2019.03.019.

[36] D. Jaganyi, M. Altaf, I. Wekesa, Synthesis and characterization of whisker-shaped MnO2 nanostructure at room temperature, Appl. Nanosci. 3 (2012) 329–333, https://doi.org/10.1007/s13204-012-0135-3.
[37] E. Cherian, A. Rajan, G. Baskar, Synthesis of manganese dioxide nanoparticles using co-precipitation method and its antimicrobial activity, Int. J. Mod. Sci. Technol. 1 (2016) 17–22.
[38] A. Muhammad, A.U.H.A. Shah, S. Bilal, Effective adsorption of hexavalent chromium and divalent nickel ions from water through polyaniline, Iron oxide, and their composites, Appl. Sci. 10 (2020) 2882, https://doi.org/10.3390/app10082882.
[39] V.-P. Dinh, M.-D. Nguyen, Q.H. Nguyen, T.-T.-T. Do, T.-T. Luu, A.T. Luu, T.D. Tap, T.-H. Ho, T.P. Phan, T.D. Nguyen, L.V. Tan, Chitosan-MnO2 nanocomposite for effective removal of Cr (VI) from aqueous solution, Chemosphere 257 (2020) 127147, https://doi.org/10.1016/j.chemosphere.2020.127147.
[40] M. Mushtaq, I.M. Tan, L. Ismail, M. Nadeem, M. Sagir, R. Azam, R. Hashmet, Influence of PZC (point of zero charge) on the static adsorption of anionic surfactants on a Malaysian sandstone, J. Dispers. Sci. Technol. 35 (2013) 343–349, https://doi.org/10.1080/01932691.2013.785362.
[41] K. Das, U. Sukul, J.-S. Chen, R.K. Sharma, P. Banerjee, G. Dey, Md. Taharia, C. J. Wijaya, C.-I. Lee, S.-L. Wang, N.H.K. Nuong, C.-Y. Chen, Transformative and sustainable insights of agricultural waste-based adsorbents for water defluoridation: biosorption dynamics, economic viability, and spent adsorbent management, Heliyon 10 (2024) e29747, https://doi.org/10.1016/j.heliyon.2024.e29747.
[42] Z. Tattibayeva, S. Tazhibayeva, W. Kujawski, B. Zayadan, K. Musabekov, Peculiarities of adsorption of Cr (VI) ions on the surface of Chlorella vulgaris ZBS1 algae cells, Heliyon 8 (2022) e10468, https://doi.org/10.1016/j.heliyon.2022.e10468.
[43] X. Li, S. Wang, Y. Liu, L. Jiang, B. Song, M. Li, G. Zeng, X. Tan, X. Cai, Y. Ding, Adsorption of cu(II), Pb(II), and cd(II) ions from acidic aqueous solutions by Diethylenetriaminepentaacetic acid-modified magnetic graphene oxide, J. Chem. Eng. Data 62 (2016) 407–416, https://doi.org/10.1021/acs.jced.6b00746.
[44] M. Li, Q. Li, L. Li, Z. Xu, J. An, G. He, Z. Wu, S. Li, W. Zhang, Crossed-linked chitosan coated cuprous oxide microspheres for iodide adsorption via one-step in-situ generation, Chin. J. Anal. Chem. (2024) 100487, https://doi.org/10.1016/j.cjac.2024.100487.
[45] A.B. Muley, M.R. Ladole, P. Suprasanna, S.G. Dalvi, Intensification in biological properties of chitosan after γ-irradiation, Int. J. Biol. Macromol. 131 (2019) 435–444, https://doi.org/10.1016/j.ijbiomac.2019.03.072.
[46] Z. Jia, C. Yang, F. Zhao, X. Chao, Y. Li, H. Xing, One-step reinforcement and deacidification of paper documents: application of Lewis Base—chitosan nanoparticle coatings and analytical characterization, Coatings 10 (2020) 1226, https://doi.org/10.3390/coatings10121226.
[47] P.C. Bandara, J. Peña-Bahamonde, D.F. Rodrigues, Redox mechanisms of conversion of Cr(VI) to Cr(III) by graphene oxide-polymer composite, Sci. Rep. 10 (2020), https://doi.org/10.1038/s41598-020-65534-8.
[48] F. Hong, P. Qiu, Y. Wang, P. Ren, J. Liu, J. Zhao, D. Gou, Chitosan-based hydrogels: from preparation to applications, a review, Food Chem.: X. 21 (2023) 101095, https://doi.org/10.1016/j.fochx.2023.101095.
[49] F. Besharat, F. Ahmadpoor, M. Nasrollahzadeh, Graphene-based (nano)catalysts for the reduction of Cr(VI): a review, J. Mol. Liq. 334 (2021) 116123, https://doi.org/10.1016/j.molliq.2021.116123.
[50] C. Ganglo, J. Rui, Q. Zhu, J. Shan, Z. Wang, F. Su, D. Liu, J. Xu, M. Guo, J. Qian, Chromium (III) coordination capacity of chitosan, Int. J. Biol. Macromol. 148 (2020) 785–792, https://doi.org/10.1016/j.ijbiomac.2020.01.203.
[51] A. Bashir, L.A. Malik, S. Ahad, T. Manzoor, M.A. Bhat, G.N. Dar, A.H. Pandith, Removal of heavy metal ions from aqueous system by ion-exchange and biosorption methods, Environ. Chem. Lett. 17 (2018) 729–754, https://doi.org/10.1007/s10311-018-00828-y.
[52] S.I. Rojas, D.C. Duarte, S.D. Mosquera, F. Salcedo, J.P. Hinestroza, J. Husserl, Enhanced biosorption of Cr(VI) using cotton fibers coated with chitosan – role of ester bonds, Water Sci. Technol. 78 (2018) 476–486, https://doi.org/10.2166/wst.2018.284.
[53] S. Fenti, P. Chianese, D. Iovino, S. Musmarra, Salvestrini, Cr(VI) sorption from aqueous solution: a review, Appl. Sci. 10 (2020) 6477, https://doi.org/10.3390/app10186477.
[54] B. Ren, Y. Jin, L. Zhao, C. Cui, X. Song, Enhanced Cr(VI) adsorption using chemically modified dormant aspergillus Niger spores: process and mechanisms, J. Environ. Chem. Eng. 10 (2021) 106955, https://doi.org/10.1016/j.jece.2021.106955.
[55] R.N. Kasavo, M. Bhaumik, H.G. Brink, Removal of chromium from aqueous solution using a nanocomposite of nickel ferrite and polyaniline doped with 2-naphthalene sulfonic acid, J. Environ. Chem. Eng. 11 (2023) 111229, https://doi.org/10.1016/j.jece.2023.111229.
[56] S. Singh, A.G. Anil, T.S.S.K. Naik, B. U, S. Khasnabis, B. Nath, V. Kumar, S. Subramanian, J. Singh, P.C. Ramamurthy, Mechanism and kinetics of Cr(VI) adsorption on biochar derived from *Citrobacter freundii* under different pyrolysis temperatures, J. Water Process Eng. 47 (2022) 102723, https://doi.org/10.1016/j.jwpe.2022.102723.
[57] F.A. Dawodu, B.M. Akpan, K.G. Akpomie, Sequestered capture and desorption of hexavalent chromium from solution and textile wastewater onto low cost *Heinsia crinita* seed coat biomass, Appl Water Sci 10 (2019), https://doi.org/10.1007/s13201-019-1114-6.
[58] V. Singh, J. Singh, V. Mishra, Development of a cost-effective, recyclable and viable metal ion doped adsorbent for simultaneous adsorption and reduction of toxic Cr (VI) ions, J. Environ. Chem. Eng. 9 (2021) 105124, https://doi.org/10.1016/j.jece.2021.105124.
[59] F. Gorzin, M.B.R. Abadi, Adsorption of Cr(VI) from aqueous solution by adsorbent prepared from paper mill sludge: kinetics and thermodynamics studies, Adsorpt. Sci. Technol. 36 (2017) 149–169, https://doi.org/10.1177/0263617416686976.
[60] E. Berhane, B. Negassa, K.T. Ayansa, D. Dadi, S. Fekadu, Cabbage waste derived activated carbon for removing hexavalent chromium from synthetic and tannery wastewater, BMC Chem. 19 (2025), https://doi.org/10.1186/s13065-025-01479-1.
[61] G.M. Ayoub, A. Damaj, H. El-Rassy, M. Al-Hindi, R.M. Zayyat, Equilibrium and kinetic studies on adsorption of chromium(VI) onto pine-needle-generated activated carbon, SN Appl. Sci. 1 (2019), https://doi.org/10.1007/s42452-019-1617-7.
[62] F.H. Emamy, A. Bumajdad, J.P. Lukaszewicz, Adsorption of hexavalent chromium and divalent lead ions on the nitrogen-enriched chitosan-based activated carbon, Nanomaterials 11 (2021) 1907, https://doi.org/10.3390/nano11081907.
[63] V. Singh, J. Singh, V. Mishra, Sorption kinetics of an eco-friendly and sustainable Cr (VI) ion scavenger in a batch reactor, J. Environ. Chem. Eng. 9 (2021) 105125, https://doi.org/10.1016/j.jece.2021.105125.
[64] C. Zheng, H. Zheng, Y. Sun, B. Xu, Y. Wang, X. Zheng, Y. Wang, Simultaneous adsorption and reduction of hexavalent chromium on the poly(4-vinyl pyridine) decorated magnetic chitosan biopolymer in aqueous solution, Bioresour. Technol. 293 (2019) 122038, https://doi.org/10.1016/j.biortech.2019.122038.
[65] T.C. Egbosiuba, A.S. Abdulkareem, A.S. Kovo, E.A. Afolabi, J.O. Tijani, M. T. Bankole, S. Bo, W.D. Roos, Adsorption of Cr(VI), Ni(II), Fe(II) and cd(II) ions by KIAgNPs decorated MWCNTs in a batch and fixed bed process, Sci. Rep. 11 (2021), https://doi.org/10.1038/s41598-020-79857-z.
[66] Y. Fang, X. Wu, M. Dai, A. Lopez-Valdivieso, S. Raza, I. Ali, C. Peng, J. Li, I. Naz, The sequestration of aqueous Cr(VI) by zero valent iron-based materials: from synthesis to practical application, J. Clean. Prod. 312 (2021) 127678, https://doi.org/10.1016/j.jclepro.2021.127678.
[67] F. Zhu, T. Liu, Z. Zhang, W. Liang, Remediation of hexavalent chromium in column by green synthesized nanoscale zero-valent iron/nickel: factors, migration model and numerical simulation, Ecotoxicol. Environ. Saf. 207 (2020) 111572, https://doi.org/10.1016/j.ecoenv.2020.111572.
[68] J. Park, J.-H. Shin, W. Oh, S.-J. Choi, J. Kim, C. Kim, J. Jeon, Removal of hexavalent chromium(VI) from wastewater using chitosan-coated Iron oxide nanocomposite membranes, Toxics 10 (2022) 98, https://doi.org/10.3390/toxics10020098.
[69] K. Choi, S. Lee, J.O. Park, J.-A. Park, S.-H. Cho, S.Y. Lee, J.H. Lee, J.-W. Choi, Chromium removal from aqueous solution by a PEI-silica nanocomposite, Sci. Rep. 8 (2018), https://doi.org/10.1038/s41598-018-20017-9.
[70] G. Lemessa, Y. Chebude, E. Alemayehu, Adsorptive removal of Cr (VI) from wastewater using magnetite–diatomite nanocomposite, AQUA — Water Infrastructure, Ecosystems and Society 72 (2023) 2239–2261, https://doi.org/10.2166/aqua.2023.132.
[71] B. Eyvazi, A. Jamshidi-Zanjani, A.K. Darban, Synthesis of nano-magnetic MnFe2O4 to remove Cr(III) and Cr(VI) from aqueous solution: a comprehensive study, Environ. Pollut. 265 (2019) 113685, https://doi.org/10.1016/j.envpol.2019.113685.
[72] A.-E. Segneanu, I.A. Bradu, M.S. Calinescu, G. Vlase, T. Vlase, D.-D. Herea, G. Buema, M. Mihailescu, I. Grozescu, Novel nanocomposites and biopolymer-based nanocomposites for hexavalent chromium removal from aqueous media, Polymers 16 (2024) 3469, https://doi.org/10.3390/polym16243469.
[73] C. Jiao, X. Tan, A. Lin, W. Yang, Preparation of activated carbon supported bead string structure nano zero valent iron in a polyethylene glycol-aqueous solution and its efficient treatment of CR(VI) wastewater, Molecules 25 (2019) 47, https://doi.org/10.3390/molecules25010047.
[74] N.K. Mondal, S. Chakraborty, Adsorption of Cr(VI) from aqueous solution on graphene oxide (GO) prepared from graphite: equilibrium, kinetic and thermodynamic studies, Appl Water Sci 10 (2020), https://doi.org/10.1007/s13201-020-1142-2.
[75] X.-L. Chen, F. Li, X.J. Xie, Z. Li, L. Chen, Nanoscale zero-valent iron and chitosan functionalized *Eichhornia crassipes* biochar for efficient hexavalent chromium removal, Int. J. Environ. Res. Public Health 16 (2019) 3046, https://doi.org/10.3390/ijerph16173046.
[76] N. Benadji, R. Ikkene, A. Boudjemaa, Z. Bendjama, K. Bachari, S. Hamoudi, Removal of Cr(VI) from aqueous solutions using amino-functionalized carbon Nanospheres adsorbents, Water Environ. Res. 90 (2018) 1925–1937, https://doi.org/10.2175/106143017x15131012188132.
[77] L. Dewa, S.M. Tichapondwa, W. Mhike, Adsorption of hexavalent chromium from wastewater using polyaniline-coated microcrystalline cellulose nanocomposites, RSC Adv. 14 (2024) 6603–6616, https://doi.org/10.1039/d3ra08027g.
[78] M.S. Samuel, J. Bhattacharya, S. Raj, N. Santhanam, H. Singh, N.D.P. Singh, Efficient removal of chromium(VI) from aqueous solution using chitosan grafted graphene oxide (CS-GO) nanocomposite, Int. J. Biol. Macromol. 121 (2018) 285–292, https://doi.org/10.1016/j.ijbiomac.2018.09.170.
[79] A.E. Shahawy, M.F. Mubarak, M.E. Shafie, H.M. Abdulla, Fe(iii) and Cr(vi) ions' removal using AgNPs/GO/chitosan nanocomposite as an adsorbent for wastewater treatment, RSC Adv. 12 (2022) 17065–17084, https://doi.org/10.1039/d2ra01612e.
[80] Z. Wan, D.-W. Cho, D.C.W. Tsang, M. Li, T. Sun, F. Verpoort, Concurrent adsorption and micro-electrolysis of Cr (VI) by nanoscale zerovalent iron/biochar/ca-alginate composite, Environ. Pollut. 247 (2019) 410–420, https://doi.org/10.1016/j.envpol.2019.01.047.

[81] J. Bayuo, M.A. Abukari, K.B. Pelig-Ba, Desorption of chromium (VI) and lead (II) ions and regeneration of the exhausted adsorbent, Appl Water Sci 10 (2020), https://doi.org/10.1007/s13201-020-01250-y.
[82] Y. He, P. Zhang, L. Wang, Adsorption and removal of Cr6+, Cu2+, Pb2+, and Zn2 + from aqueous solution by magnetic Nano-chitosan, Molecules 28 (2023) 2607, https://doi.org/10.3390/molecules28062607.
[83] X. Du, C. Kishima, H. Zhang, N. Miyamoto, N. Kano, Removal of chromium(VI) by chitosan beads modified with sodium dodecyl sulfate (SDS), Appl. Sci. 10 (2020) 4745, https://doi.org/10.3390/app10144745.